

Annual Review of Condensed Matter Physics Understanding Hydrophobic Effects: Insights from Water Density Fluctuations

Nicholas B. Rego and Amish J. Patel

Department of Chemical and Biomolecular Engineering, University of Pennsylvania, Philadelphia, Pennsylvania, USA; email: amish.patel@seas.upenn.edu

Annu. Rev. Condens. Matter Phys. 2022. 13:303-24

First published as a Review in Advance on November 23, 2021

The Annual Review of Condensed Matter Physics is online at commatphys.annualreviews.org

https://doi.org/10.1146/annurev-conmatphys-040220-045516

Copyright © 2022 by Annual Reviews. All rights reserved

ANNUAL CONNECT

www.annualreviews.ora

- · Download figures
- Navigate cited references
- Keyword search
- Explore related articles
- · Share via email or social media

Keywords

solvation, contact angle, aqueous self-assembly, protein folding, biomolecular interactions, supramolecular chemistry, dewetting

Abstract

The aversion of hydrophobic solutes for water drives diverse interactions and assemblies across materials science, biology, and beyond. Here, we review the theoretical, computational, and experimental developments that underpin a contemporary understanding of hydrophobic effects. We discuss how an understanding of density fluctuations in bulk water can shed light on the fundamental differences in the hydration of molecular and macroscopic solutes; these differences, in turn, explain why hydrophobic interactions become stronger upon increasing temperature. We also illustrate the sensitive dependence of surface hydrophobicity on the chemical and topographical patterns the surface displays, which makes the use of approximate approaches for estimating hydrophobicity particularly challenging. Importantly, the hydrophobicity of complex surfaces, such as those of proteins, which display nanoscale heterogeneity, can nevertheless be characterized using interfacial water density fluctuations; such a characterization also informs protein regions that mediate their interactions. Finally, we build upon an understanding of hydrophobic hydration and the ability to characterize hydrophobicity to inform the context-dependent thermodynamic forces that drive hydrophobic interactions and the desolvation barriers that impede them.

1. INTRODUCTION

Hydrophobic effects, which refer to the aversion of nonpolar solutes for water or the affinity of such solutes for one another in aqueous solutions, play an important role in diverse disciplines, ranging from interfacial science and supramolecular chemistry to soft matter and biophysics (1–6). For example, amphiphilic molecules or particles, which possess both nonpolar and polar regions, can ameliorate unfavorable interactions between oil and water, thereby giving rise to detergency and stabilizing emulsions (7, 8). Furthermore, given that half the naturally occurring amino acids are nonpolar, the hydrophobic effect also drives numerous biomolecular interactions and assemblies (9–12). The central challenge in understanding hydrophobic hydration, characterizing hydrophobicity, and anticipating hydrophobic interactions lies in capturing how hydrophobic solutes perturb water structure in their vicinity. Being a highly cohesive liquid, water tries to minimize the disruption of its structure by collectively reorganizing its hydrogen bonding network (13); however, the extent to which it succeeds can depend in nontrivial ways on solute properties, such as its size, shape, curvature, and the arrangement of its chemical groups.

In this review, we discuss the fundamental insights that underpin a contemporary understanding of hydrophobic effects. Foremost among them is the dependence of hydrophobic hydration on solute size. In particular, because water can hydrogen bond around subnanometer hydrophobic solutes, but not around larger solutes, molecular and macroscopic solutes perturb water structure differently (14). An understanding of density fluctuations in bulk water can shed light on these differences, explaining how the hydration free energy of a small solute is dominated by the entropic cost of constraining the hydrogen bond network of its hydration waters and scales as solute volume, whereas the hydration free energy of a large solute is dominated by the enthalpic cost of broken hydrogen bonds in its hydration shell and scales as its surface area (13). Similarly, an understanding of water density fluctuations in the vicinity of a surface serves to characterize its hydrophobicity. In particular, the free energetic cost of displacing interfacial waters to create a cavity next to a surface provides a general, unambiguous measure of its hydrophobicity; the easier it is to create an interfacial cavity, the more hydrophobic the surface (15-19). Such a measure can also be used to estimate the hydrophobicity of complex surfaces, such as those of proteins, which display chemical and topographical heterogeneity at the nanoscale. The use of interfacial fluctuations to characterize the hydrophobicity of complex surfaces has highlighted that hydrophobicity can be remarkably sensitive to curvature and chemical patterning (20–24), and that approximate approaches for estimating hydrophobicity, based on surface area or additivity, are doomed to fail for all but the simplest of systems (25-28). We then discuss how an understanding of hydrophobic hydration and the ability to characterize hydrophobicity inform the thermodynamic forces that drive hydrophobic interactions and assemblies (29, 30). We also discuss how water density fluctuations in confinement between hydrophobic solutes can influence the kinetics and pathways of hydrophobic assembly (31–36).

Throughout, we draw on insights obtained from theoretical and computational studies and make connections to experiments. As with any vibrant field, our understanding of hydrophobic effects has been shaped by numerous dedicated researchers and countless insightful studies. Regrettably, we are unable to discuss many important findings here, including several that have inspired our work and shaped our outlook on the subject. Fortunately, we are able to point the interested reader to a number of recent reviews, which focus on different aspects of hydrophobic effects and serve as excellent complements to our discussion here (2–5, 37–40).

2. HYDRATION OF SMALL AND LARGE HYDROPHOBIC SOLUTES

When a hydrophobic solute is hydrated, i.e., transferred to water from vapor or oil (**Figure 1***a*), it disrupts the inherent structure of water (41, 42). Water molecules in the vicinity of the solute

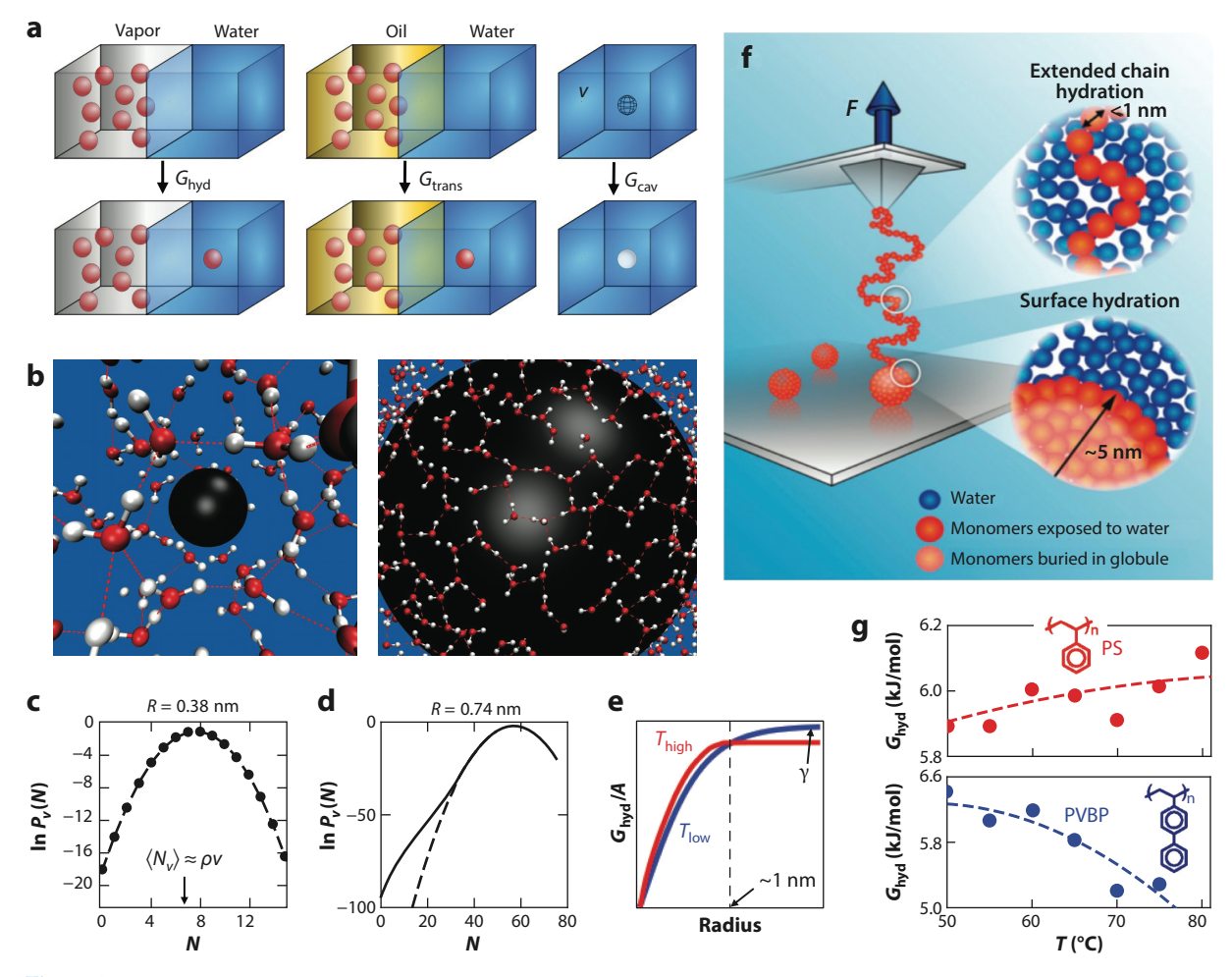


Figure 1

Hydrophobic hydration, density fluctuations in bulk water, and solute size-dependent crossover. (a) The hydration (i.e., dissolution in water from vapor or oil) of a nonpolar solute (red sphere) disrupts water structure in ways that are remarkably similar to the creation of a cavity by emptying a solute-sized volume, v, in bulk water. (b) The hydrogen bond network of water is strained but remains intact near small solutes, such as methane (left); in contrast, water is unable to form four hydrogen bonds near extended hydrophobic solutes (right). (c) The probability, $P_v(N)$, of observing N waters in small observation volumes, v, which contain only a few waters on average, is Gaussian (dashed line) for all N(13, 45). (d) For larger probe volumes, although $P_v(N)$ is Gaussian near the mean, low-N fluctuations are enhanced (13, 16). (e) Schematic illustrating that the hydration free energy, G_{hvd} , of small spherical solutes scales with their volume, whereas for large solutes, G_{hyd} is determined by interfacial physics and scales with solute area, A; the crossover between the two regimes occurs at a solute size of roughly 1 nm (13, 14). Furthermore, small solute hydration is entropically unfavorable, so Ghyd increases as temperature is increased from T_{low} (blue) to T_{high} (red); in contrast, for large solutes, G_{hvd} decreases as temperature is increased. (f) By using an AFM tip to pull on polymers, Li & Walker (48) forcibly hydrated hydrophobic monomers; the requisite force informed the monomer hydration free energy. (g) Hydration free energies, G_{hvd} , are shown as a function of temperature for two monomer side chains. For the smaller monomer, G_{hvd} increases with T(top), whereas for the larger monomer, it decreases above 50°C (bottom; 48). Panel b adapted with permission from Reference 14; copyright 2005 Springer Nature. Panel c adapted with permission from Reference 45; copyright 1996 National Academy of Sciences and with permission from Reference 13; copyright 2012 Società Italiana di Fisica. Panel d adapted with permission from Reference 16; copyright 2010 American Chemical Society and with permission from Reference 13; copyright 2012 Società Italiana di Fisica. Panel e adapted with permission from Reference 14; copyright 2005 Springer Nature and with permission from Reference 13; copyright 2012 Società Italiana di Fisica. Panels f and g adapted with permission from Reference 48; copyright 2011 National Academy of Sciences. Abbreviations: AFM, atomic force microscopy; PS, polystyrene; PVBP, poly(4-vinylbiphenyl).

try to minimize this disruption by collectively reorganizing their hydrogen bonding network; however, the extent to which they succeed depends in interesting and nontrivial ways on the size and shape of the hydrophobic solute. It is this collective reorganization of hydration waters, and its complex dependence on solute properties, that confers hydrophobic effects with their many exotic properties.

2.1. How Water Responds to Molecular and Macroscopic Hydrophobic Solutes

The manner in which molecular and macroscopic hydrophobic solutes perturb water structure is fundamentally different (**Figure 1***b*). Water molecules near a small nonpolar solute, such as methane, are able to maintain all their hydrogen bonds. However, accommodating the solute severely constrains the hydrogen bonding network of its hydration waters and results in a large negative entropy of hydration (14). In contrast, the hydration waters of a macroscopic hydrophobic solute, such as a colloidal particle, are simply incapable of participating in four hydrogen bonds like those in bulk water; instead, they sacrifice a hydrogen bond in the same way that water molecules do at a water–vapor interface (43, 44). Given these fundamental differences in the hydration of molecular and macroscopic solutes, how do we characterize the extent to which diverse hydrophobic solutes perturb water structure in their vicinity? The answer to this question lies in an understanding of density fluctuations in bulk water; fluctuations provide a quantitative framework for characterizing the disruption of water structure by hydrophobic solutes and for informing their hydration free energies (45–47).

2.2. Water Density Fluctuations Inform Hydrophobic Hydration

Nonpolar solutes exclude water molecules from the regions they occupy and attract their hydration waters through dispersive interactions; however, the latter are relatively weak and do not perturb water structure substantially (49). Consequently, hard solutes or cavities, which simply exclude water molecules (**Figure 1a**), have been extensively studied as idealized hydrophobic solutes (50–52). Importantly, because hydrating a hard solute or creating a cavity is equivalent to emptying a solute-sized volume v, the hydration free energy of idealized solutes is given by $G_{\text{cav}} = -k_{\text{B}}T \ln P_v(N \to 0)$, where k_{B} is Boltzmann's constant, T is temperature, and $P_v(N)$ is the probability of observing N waters in v (53, 54).

Using molecular simulations, Hummer et al. (45) showed that the statistics of water number fluctuations, $P_v(N)$, in small observation volumes are Gaussian for all N; i.e.,

$$P_v(N) pprox rac{1}{\sqrt{2\pi\sigma^2}} \cdot \expigg[-rac{(N-\langle N_v
angle)^2}{2\sigma^2}igg],$$
 1.

where $\langle N_v \rangle = \rho v$ and $\sigma^2 \equiv \langle \delta N_v^2 \rangle$ are the mean and variance of $P_v(N)$, respectively, and ρ is the density of bulk water (**Figure 1**c). Along with famed theoretical developments, such as the Percus-Yevick theory of hard spheres and the Pratt–Chandler theory of hydrophobic hydration, the above finding is underpinned by the fact that in a dense fluid, small fluctuations in density obey Gaussian statistics (55–57). Importantly, it led to a relationship between $G_{\rm cav}$ and the moments of $P_v(N)$ (45, 46):

$$G_{\rm cav} pprox k_{\rm B}T \left[rac{
ho^2 v^2}{2\sigma^2} + rac{1}{2} \ln(2\pi\sigma^2)
ight] pprox rac{k_{\rm B}T}{2} \cdot rac{
ho^2 v^2}{\sigma^2}.$$

To a reasonable approximation, $\sigma^2 = \langle \delta N_v^2 \rangle \propto \langle N_v \rangle \propto v$. Thus, $G_{\rm cav} \propto v^2/\sigma^2 \propto v$; i.e., the free energy for hydrating small hydrophobic solutes scales as solute volume, v. Equation 2 also provides a way to understand the temperature dependence of $G_{\rm cav}$. Garde et al. (46) showed that σ^2

depends weakly on T, so that $G_{cav} \sim T\rho^2$, which increases with T at ambient conditions. These arguments provide a way to understand why the solubility of noble gases in water decreases with increasing temperature. They also imply a negative entropy, S_{cav} , for hydrating small hydrophobic solutes, which is consistent with the constrained hydrogen bonding network of their hydration waters.

For large volumes in bulk water, $P_v(N)$ remains Gaussian near its mean, but the likelihood of observing low-N fluctuations is enhanced significantly (**Figure 1**d; 16, 47). The enhanced low-N fluctuations are a consequence of the proximity of water at ambient conditions to liquid–vapor coexistence, so that once a certain number of waters leave v, it becomes easier to further dewet the volume by nucleating a vapor bubble (58, 59). The dewetting of large volumes is thus governed by interfacial physics, and the free energetic cost of lowering N below a certain threshold is roughly γA , where γ is the water–vapor surface tension and A is the surface area of the vapor bubble; i.e., $-\ln P_v(N) \propto \gamma (v - N/\rho)^{2/3}$, where $(v - N/\rho)$ is the bubble volume. Consequently, for large solutes, $G_{\text{cav}} \propto \gamma v^{2/3}$, and because γ decreases with increasing T, so does G_{cav} . In contrast with small solutes, S_{cav} is thus positive for large hydrophobic solutes (60).

2.3. Solute Size-Dependent Crossover in Hydrophobic Hydration Free Energies

Given the fundamental differences in the hydration of small and large hydrophobic solutes, at what solute size does the crossover occur from molecular solutes, whose hydration free energies scale with solute volume, to macroscopic solutes, whose hydration free energies scale with surface area? Molecular simulations and theory have shown that the crossover occurs at a solute size of roughly 1 nm (**Figure 1e**; 59–62). Interestingly, the building blocks of typical molecular assemblies, e.g., amino acid side chains, tend to be smaller than 1 nm, whereas the corresponding assemblies, e.g., folded proteins, are usually larger than 1 nm. Thus, to capture the driving forces for diverse self-assembly phenomena, e.g., micelle formation or protein folding, and to rationalize why those driving forces increase with temperature (Section 5.1), it is critical to understand the physics of hydrophobic hydration as it crosses over from one regime to another and also to be able to quantitatively characterize the corresponding free energies. To this end, the physics of both Gaussian fluctuations and interface formation have been encoded in the Lum–Chandler–Weeks theory of hydrophobicity (59) as well as in the theoretical contributions it has motivated (63–66).

2.4. Experimental Evidence of Crossover in Hydrophobic Hydration

Theory and molecular simulations played an important role in elucidating the differences in the hydration of small and large hydrophobic solutes; however, experimental verification of these ideas was complicated by the fact that small nonpolar solutes are only sparingly soluble in water, and their solubility decreases precipitously as solute size increases. To address this challenge, Davis et al. (67) studied the hydration shells of a family of linear alcohols, increasing in size from methanol to heptanol, over a wide range of temperatures from 0–100°C. By using Raman scattering measurements with multivariate curve resolution, the authors found that the hydration shells of small alcohols displayed signatures of enhanced tetrahedral order, whereas the hydration shells of longer alcohols were relatively disordered, supporting the notion that the disruption of water structure near small and large hydrophobic solutes is fundamentally different. In another creative study, Li & Walker (48) used single-molecule force spectroscopy to investigate the hydration of several hydrophobic polymers with nanoscopic side chains of different sizes. Although the hydrophobic polymers collapse and crash out of the aqueous solution, as expected, the

authors forcibly hydrated their monomers by using an atomic force microscopy (AFM) tip to pull on individual polymers (**Figure 1**f). By measuring the force required to unravel the polymers, the authors were then able to estimate the free energy of hydrating the monomers, G_{hyd} . For the smallest monomer studied, G_{hyd} increased with temperature, whereas for the largest monomer, G_{hyd} decreased above 50°C (**Figure 1**g). These findings provide strong experimental support for the solute size–dependent crossover in the physics of hydrophobic hydration and confirm that the crossover length scale near ambient conditions is roughly 1 nm (68).

3. CHARACTERIZING HYDROPHOBICITY

A characterization of solute hydrophobicity, which quantifies how strongly water structure is perturbed by the solute, can inform the strength of hydrophobic interactions (69); the more hydrophobic a solute, the more strongly it ought to bind other hydrophobic solutes. Below, we first introduce canonical metrics of hydrophobicity before introducing modern measures that are rooted in interfacial water density fluctuations; the latter can be used to estimate the hydrophobicity of heterogeneous, amphiphilic solutes (Section 4) and inform their interactions and assemblies (Section 5).

3.1. Molecular Versus Macroscopic Solutes

Because the manner in which small and large solutes perturb water is fundamentally different, it stands to reason that their hydrophobicities should also be characterized differently. The hydrophobicity of molecular solutes is typically characterized using solubility from the gas phase or partitioning from an oil phase, or equivalently, using the corresponding free energies, G_{hvd} or G_{trans} , respectively; the larger the value of G_{hvd} , the more hydrophobic the solute (**Figure 2**a; 70, 71). As discussed in Section 2.2, $G_{\rm hvd}$ is closely related to the corresponding cavity hydration free energy, G_{cav} , which is informed by density fluctuations in bulk water. Indeed, by recognizing that $P_{\nu}(N)$ in molecular volumes is Gaussian, and using it to estimate the $G_{\rm cav}$ of n-butane conformers, Hummer et al. (45) were able to show that the more compact cis conformation is favored over its trans conformation, in agreement with the corresponding estimates of G_{hvd} (72). Furthermore, trends in G_{hvd} can also shed light on the interactions and assemblies of molecular solutes, as we discuss in Section 5.1. In contrast with small solutes, the hydrophobicity of large solutes (or surfaces) is determined by interfacial physics. Below, we describe several different but related ways of characterizing hydrophobicity using interfacial physics; in Sections 5.3 and 5.4, we then illustrate how such characterizations inform the interactions between diverse extended solutes, ranging from flat, homogeneous surfaces to the rugged, heterogeneous surfaces of proteins.

3.2. Water Droplet Contact Angles and Wetting Coefficients

The hydrophobicity of a solid surface can be quantified by bringing a water droplet into contact with the surface and estimating the corresponding contact angle, θ (73). A water droplet beads up to minimize contact with hydrophobic surfaces, whereas it spreads on hydrophilic surfaces (**Figure 2b**). The contact angle is also related to the wetting coefficient, k, which quantifies the relative preference of a surface for liquid water over water vapor. In particular, $k \equiv (\gamma_{SV} - \gamma_{SL})/\gamma$, where γ_{SV} and γ_{SL} represent solid-vapor and solid-liquid surface tensions, respectively; interfacial physics stipulates that k must be equal to $\cos \theta$ (74). Thus, the hydrophobicity of flat, homogeneous surfaces can be quantified using either θ or k. However, such characterization cannot be performed for rugged, heterogeneous surfaces, such as those of proteins, which nevertheless use hydrophobic regions to interact with their binding partners (75).

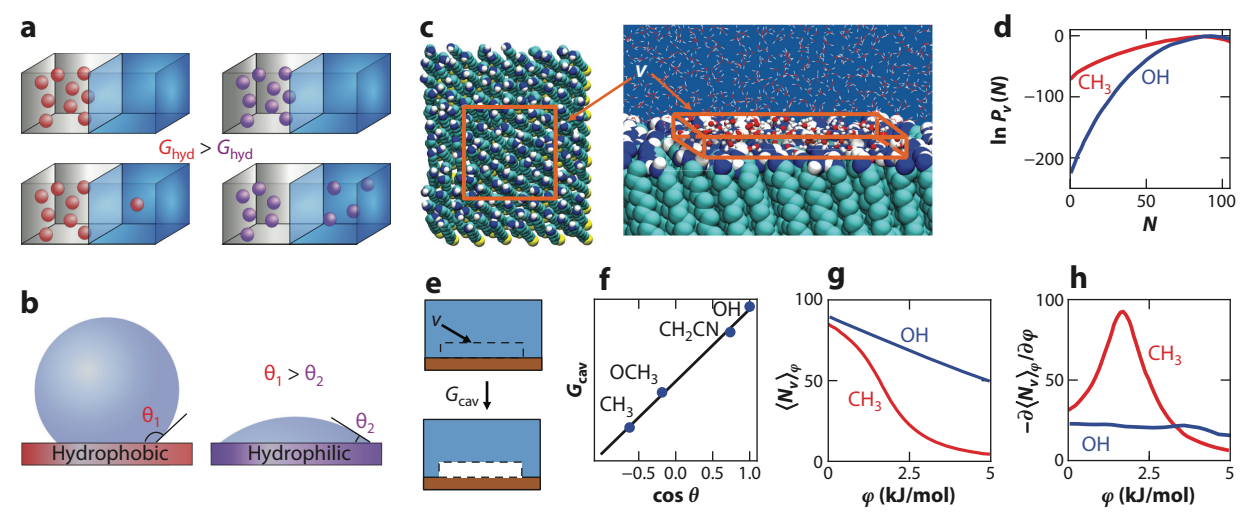


Figure 2

Characterizing hydrophobicity, water density fluctuations near surfaces, and interfacial dewetting. (a) The hydrophobicity of molecular hydrophobic solutes (red and purple spheres) is often characterized using their solubility in water or, equivalently, their hydration free energy, $G_{\rm hyd}$. (b) In contrast, the hydrophobicity of macroscopic surfaces is typically characterized using the water droplet contact angle, θ ; water beads up on hydrophobic surfaces, but spreads on hydrophilic ones. (c) Surface hydrophobicity is also reflected in the statistics of water density fluctuations, $P_v(N)$, in thin interfacial observation volumes; a cuboidal v (orange) of width 0.3 nm and cross-sectional area 3×3 nm² is shown here adjacent to an OH-terminated SAM surface. (d) Near the polar (OH-terminated) SAM surface, $P_v(N)$ is roughly Gaussian for all N, whereas near the nonpolar (CH3-terminated) SAM surface, enhanced low-N fluctuations are observed, reflecting the relative ease with which the hydrophobic surface can be dewetted. (e, f) The free energy required to create a cavity, $G_{\rm cav}$, next to a SAM surface varies linearly with $\cos\theta$ and can be used to quantify surface hydrophobicity. (g) In response to an unfavorable potential, ϕN_v , the average number of interfacial waters, $\langle N_v \rangle_{\phi}$ decreases linearly near the polar surface, whereas $\langle N_v \rangle_{\phi}$ decreases in a sigmoidal manner near the nonpolar surface. (b) Correspondingly, the susceptibility, $-\partial \langle N_v \rangle_{\phi} / \partial \phi$, displays a marked peak near the nonpolar SAM surface, suggesting that water near hydrophobic surfaces is situated at the edge of a collective dewetting transition and is particularly susceptible to unfavorable perturbations. Panels d, g, and b adapted with permission from Reference 18; copyright 2012 American Chemical Society. Panel f adapted with permission from Reference 17; copyright 2011 National Academy of Sciences. Abbreviation: SAM, self-assembled monolayer.

Once again, an understanding of water density fluctuations, this time in the vicinity of surfaces, provides the insights needed to address this challenge.

3.3. Water Density Fluctuations at Extended Surfaces

To illustrate the relationship between surface hydrophobicity and interfacial water density fluctuations, we compare and contrast the statistics of water number fluctuations, $P_v(N)$, in thin interfacial volumes, v, adjacent to self-assembled monolayer (SAM) surfaces, terminated with either methyl (-CH₃) or hydroxyl (-OH) groups (**Figure 2c**; 18). Although the average number of interfacial water molecules is similar in both cases, there are marked differences in the two $P_v(N)$ curves at low N (**Figure 2d**). For the nonpolar CH₃-terminated SAM surface, the likelihood of low-N fluctuations is enhanced significantly relative to the polar OH-terminated SAM surface. Thus, the free energetic cost of displacing a sufficient fraction of interfacial waters is lower near a hydrophobic surface than a hydrophilic surface. In other words, the ease with which surface—water interactions can be disrupted, by dewetting interfacial volumes, depends on how weak those interactions were to begin with.

3.4. Interfacial Cavity Hydration Free Energy as a Measure of Hydrophobicity

Because dewetting hydrophobic surfaces is easier than hydrophilic ones, the free energy required to create a cavity near a surface, G_{cav} , can serve as a measure of surface hydrophobicity. Furthermore, G_{cav} can also be related to conventional measures of hydrophobicity, such as θ , using interfacial physics. In particular, $G_{\text{cav}} \approx (\gamma + \gamma_{\text{SV}} - \gamma_{\text{SL}})A_{\text{c}}$, where A_{c} is the cross-sectional area of v (Figure 2e); Young's equation then suggests a linear relationship between G_{cav} and $\cos \theta$; i.e., $G_{\rm cav} \approx (1 + \cos \theta) \gamma A_{\rm c}$. Patel et al. (17) estimated $G_{\rm cav}$ for a family of SAM surfaces with different end groups, which confer upon the surfaces a wide range of hydrophobicities, and found that G_{cav} indeed varies linearly with $\cos\theta$ (Figure 2f). Thus, the hydrophobicity of flat surfaces can be equivalently characterized using either θ or G_{cav} . Importantly, the connection between G_{cav} and $\cos \theta$ suggests that even when θ is ill defined, e.g., for complex surfaces such as those of proteins, G_{cav} can nevertheless be used to characterize hydrophobicity (15, 17). In addition to enhanced interfacial water density fluctuations, and the corresponding ease of cavity creation, the disruption of water structure near hydrophobic surfaces is also reflected in other interfacial properties, such as isothermal compressibility, transverse density correlations, distribution of water dipole orientations, interfacial diffusivity, orientational relaxation times, hydrodynamic slip, and Kapitza resistance (15, 43, 76–80). Like G_{cav} , some of these quantities have also been employed as reporters of surface hydrophobicity and used to interrogate surfaces with nanoscale complexity (20, 22, 81–86).

3.5. Response of Interfacial Waters to Unfavorable Perturbations

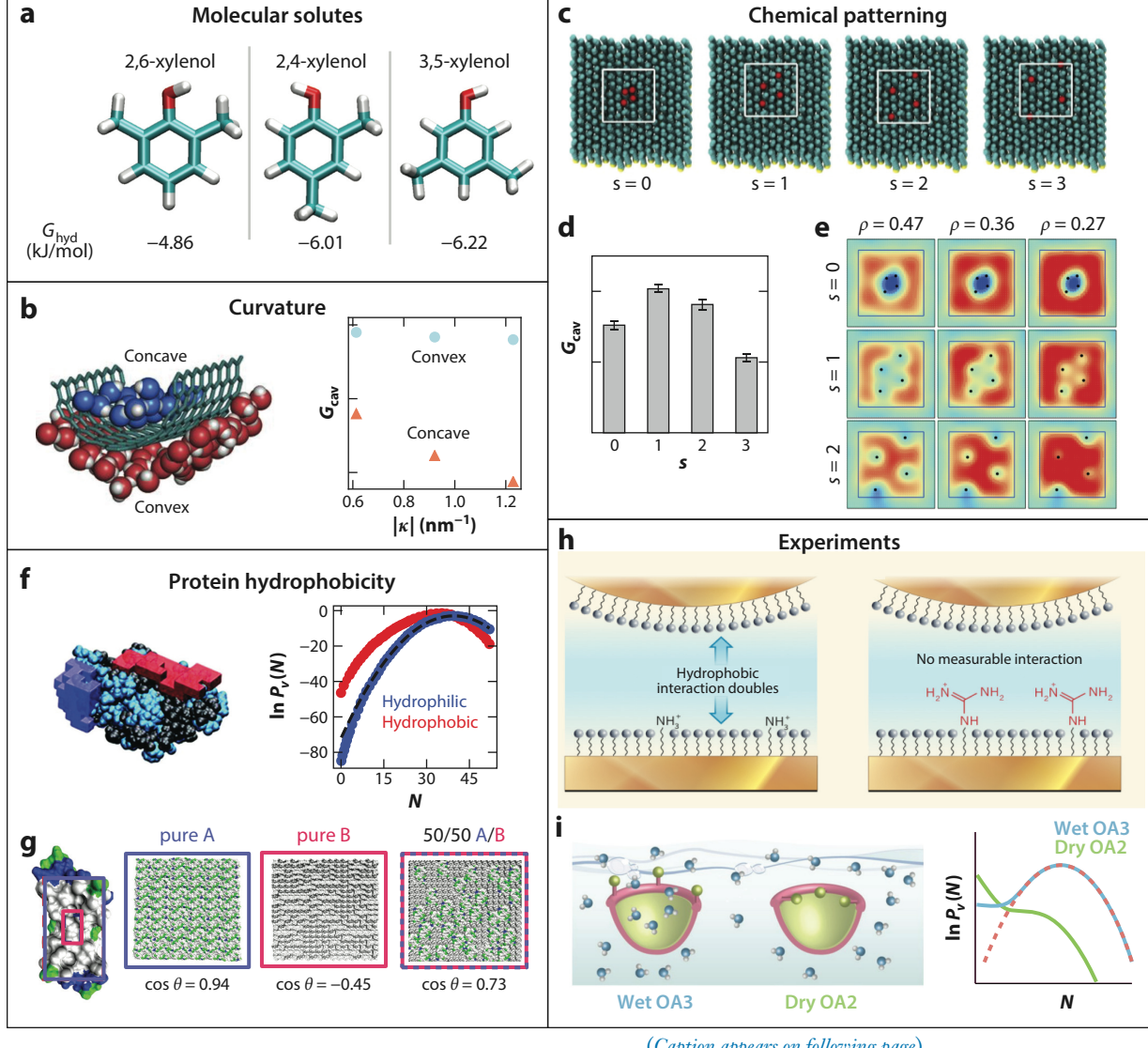
In addition to serving as descriptors of surface hydrophobicity, the rare low-N tails of interfacial water density fluctuations (Figure 2d) also dictate the response of interfacial waters to unfavorable perturbations, e.g., interfacial dewetting facilitated by the approach of a binding partner (Sections 6.3 and 6.4; 32, 33), the addition of a cosolvent (87), etc. In particular, consider the contrasting response of water near hydrophobic and hydrophilic surfaces to an unfavorable linear potential, ϕN_v , where ϕ represents the potential strength and N_v is the number of waters in the interfacial volume, v. As ϕ is increased, the average number of waters, $\langle N_v \rangle_{\phi}$, near the OH-terminated SAM surface decreases gradually (linear response); in contrast, near the CH₃terminated SAM surface, $\langle N_v \rangle_{\phi}$ displays a sharp decrease (**Figure 2g**; 18, 88). Correspondingly, the susceptibility, $-\partial \langle N_v \rangle_{\phi}/\partial \phi$, displays a peak near the hydrophobic surface (**Figure 2b**). Such a peak in susceptibility is a well-known feature of phase transitions and is a direct consequence of enhanced low-N fluctuations (18). Thus, low-N fat tails in the statistics, $P_v(N)$, of interfacial water density fluctuations situate interfacial waters at the edge of a dewetting transition and render them sensitive to unfavorable perturbations. Interestingly, the susceptibility of interfacial waters to unfavorable perturbations also manifests itself in the remarkable sensitivity of G_{cav} to the characteristics of a hydrophobic surface. Indeed, as we see in Section 4, small differences in surfaces cues, such as curvature, substitution of individual chemical groups (e.g., mutations), or rearrangement of moieties (patterning), can all substantially modulate G_{cav} and, thereby, surface hydrophobicity. In contrast, hydrophilic surfaces tend to be relatively insensitive to subtle changes in surface properties (22).

4. HETEROGENEOUS SOLUTES: HYDROPHOBICITY IN CONTEXT

The most interesting solutes that participate in hydrophobic interactions tend to be amphiphilic; polar regions facilitate their hydration, whereas nonpolar regions facilitate their interactions. The extent to which water structure is perturbed by such heterogeneous solutes depends on their detailed chemical and topographical patterns in ways that can be both surprising and nonintuitive.

4.1. Small Amphiphilic Solutes

The hydrophobicity of a small amphiphilic solute, as quantified by G_{hyd} , depends not just on the chemical groups present in the solute but also on their spatial positions with respect to one another. For example, consider three different xylenol molecules, highlighted by Fennell & Dill (25), that have the exact same number and types of chemical groups; the solutes differ only in the locations of their methyl groups (Figure 3a). Both common intuition and more involved group additivity approaches would predict that these three compounds have similar, if not identical, hydration free energies. Instead, experiments show that 3,5-xylenol is more than twice as soluble in water as 2,6xylenol. This example highlights that the extent to which a solute perturbs water structure, and therefore its hydrophobicity, can depend sensitively on the chemical and topographical cues that



(Caption appears on following page)

Figure 3 (Figure appears on preceding page)

Context-dependent hydrophobicity of heterogeneous solutes and surfaces. (a) The hydrophobicity of xylenol isomers, as quantified by their hydration free energies, depends on the arrangement of their chemical groups with respect to one another. (b) The hydrophobicity of hemi-cylindrical surfaces, as quantified by the free energetic cost of creating interfacial cavities, G_{cav} , depends on their curvature; concave surfaces are more hydrophobic than convex ones. (c,d) For a family of SAM patches containing four -OH groups (magenta) separated by $s \in [0, 3]$ CH₃ groups (cyan), G_{cav} varies nonmonotonically with s. (e) As water is displaced from the observation volume v (white squares in panel c), wet (blue) and dry (red) patches appear in v and are shown for select partially dewetted states (ρ is the normalized water density in v). (f) The statistics of interfacial water density fluctuations, $P_v(N)$, near a hydrophobic patch (red) on the BphC enzyme (cyan, black) display low-N fat tails, whereas $P_v(N)$ near a hydrophilic protein patch (blue) is approximately Gaussian. (g) Wang et al. (27) constructed mixed surfaces using hydrophilic (blue, A) and hydrophobic (red, B) regions of the melittin protein and found that the mixed surfaces were substantially more hydrophilic than expected by additivity. (b) Ma et al. (93) demonstrated that the attraction between a hydrophobic AFM tip and an amphiphilic SAM surface increased in strength when polar amine groups were replaced with charged ammonium groups, but disappeared altogether when they were replaced by similarly charged guanidinium groups. (i) Barnett et al. (94) showed that the orientation of methyl groups (green spheres) on otherwise identical octa acid cavitands, OA3 and OA2, had a dramatic effect on their hydration, stabilizing either a wet or dry state. Panel a adapted with permission from Reference 25; copyright 2011 Springer Nature. Panels b-e adapted with permission from Reference 24; copyright 2017 National Academy of Sciences. Panel f adapted with permission from Reference 18; copyright 2012 American Chemical Society. Panel g adapted with permission from Reference 27; copyright 2011 National Academy of Sciences. Panel b adapted with permission from Reference 95; copyright 2015 Springer Nature. Panel i adapted with permission from Reference 96; copyright 2020 Springer Nature. Abbreviations: AFM, atomic force microscopy; SAM, self-assembled monolayer.

the solute presents to its hydration waters. Such sensitivity has motivated approaches that make use of the inhomogeneous water density distribution near a solute to approximately estimate its G_{hvd} (89–92).

4.2. Curved and Chemically Patterned Surfaces

As discussed in Section 3.4, the hydrophobicity of heterogeneous surfaces, which display nanoscale curvature and/or chemical patterning, can be characterized using the free energy, G_{cav} , of creating an interfacial cavity. Xi et al. (24) quantified G_{cav} near both concave and convex hemicylindrical surfaces with nanoscale curvatures and found that interfacial waters could be displaced to form cavities more readily near concave surfaces than near convex surfaces of the same curvature (**Figure 3b**). Thus, concave nonpolar surfaces are more hydrophobic than convex ones. The authors also found that concave and convex curvatures do not influence hydrophobicity in similar ways; the hydrophobicity of concave surfaces increased with curvature, whereas that of convex surfaces was relatively insensitive to curvature. Along these lines, Mittal & Hummer (23) found that rough surfaces, which possess both concave and convex curvatures, tend to be more hydrophobic than flat ones.

Xi et al. (24) also studied chemically patterned SAM patches containing a small fraction of polar groups in an otherwise nonpolar background; varying the separation, s, between adjacent polar groups led to four different patterns (**Figure 3**c). The authors found that surface hydrophilicity, as quantified by G_{cav} , was not only different for the different surfaces but varied nonmonotonically with s (**Figure 3**d). A visualization of the corresponding dewetting pathways provided a striking illustration of the collective response of the SAM hydration waters to the chemical context presented by the different patches (**Figure 3**e). Along these lines, Acharya et al. (22) found that adding a polar group to a nonpolar surface suppresses its hydrophobicity substantially, but adding a nonpolar group to a polar surface does not correspondingly enhance surface hydrophobicity. Similarly, Giovambattista et al. (21) found that inverting the polarity of silica surfaces modulates their hydrophobicity. These examples highlight that seemingly similar surfaces with identical chemical compositions, but with subtle variations in chemical patterning and/or topography, can display substantial differences in their aversion to water.

4.3. Protein Hydrophobicity

Protein surfaces display nanoscale chemical and topographical patterns, which perturb water structure in complex ways that are not easy to anticipate (97, 98). Patel et al. (18) showed that, in spite of these complexities, water density fluctuations can be used to characterize the hydrophobicity of heterogeneous protein surfaces. In particular, the authors showed that $P_v(N)$ can display low-N fat tails near hydrophobic protein regions and tends to be Gaussian near hydrophilic regions (**Figure 3**f). Similarly, Rego et al. (99) found that the hydration shells of diverse proteins were susceptible to unfavorable perturbations, suggesting that protein hydrophobicity ought to be sensitive to its chemical and topographical context. Indeed, Xi et al. (24) showed that the hydrophobicity of a protein patch, as quantified by G_{cav} , can be modulated substantially by swapping the positions of two residues in the patch. Similarly, Wang et al. (27) studied mixed surfaces comprised of polar and nonpolar regions of the melittin protein and found that polar patches disproportionately suppress surface hydrophobicity (**Figure 3**g). Finally, Rego et al. (30) classified protein regions according to their ease of dewetting and found that hydrophobic and hydrophilic patches had remarkably similar chemical compositions and contained comparable numbers of nonpolar and polar atoms.

4.4. Experimental Demonstrations of Context-Dependent Hydrophobicity

Ma et al. (93) characterized the hydrophobicity of heterogeneous surfaces by measuring the adhesive force between a hydrophobic AFM tip and the surface of interest; the stronger the force, the more hydrophobic the surface. By studying binary SAM surfaces, composed of a 60/40 mixture of -CH₃ and cationic end groups, the authors showed that surface hydrophobicity displayed a mystifying dependence on both the nature of the cationic groups and their charge (Figure 3b). Surprisingly, surfaces with cationic ammonium ions were found to be nearly twice as hydrophobic as surfaces with uncharged amine groups. Even more surprisingly, surfaces with the cationic guanidinium ions were found to be hydrophilic; i.e., they were not attracted to the hydrophobic AFM tip. In another interesting study, Barnett et al. (94) studied synthetic nanoscale bowl-shaped hosts or cavitands, which are lined with hydrophilic acid groups on the outside, to make them water soluble, and hydrophobic groups on the inside. By studying variants of the octa acid (OA) cavitands, which differ only in the orientation of the methyl groups at the rim of the bowl, i.e., the methyls point inward (OA2) or upward (OA3), the authors found that the OA3 bowl was wet, whereas the OA2 bowl was dry (Figure 3i). Molecular simulations shed further light on these interesting observations, highlighting the presence of a low-N fat tail in the $P_v(N)$ for OA3, which suggests that although OA3 is wet, it is situated at the edge of a dewetting transition. Presumably, the subtle change in the orientation of the methyl groups in going from OA3 to OA2 was then sufficient to trigger dewetting.

4.5. Shortcomings of Surface Area Models and Additive Approaches

The importance of hydrophobic interactions in driving diverse self-assembly processes has inspired numerous schemes for the efficient but approximate characterization of solute hydrophobicity. For example, surface area models (100–102) assume that the hydrophobicity of an exposed nonpolar patch is proportional to its surface area. However, the hydration of small hydrophobic solutes is governed not by interfacial physics but by the entropic constraints on their hydration waters (Section 2.2). Even for extended solutes, hydrophobicity can depend on surface curvature, particularly for concave surfaces (Section 4.2). These shortcomings of surface area models necessitate the use of an effective surface tension, whose value can depend sensitively

on the class of solutes used to estimate it (103). Another popular class of approximate approaches for characterizing protein hydrophobicity uses a divide-and-conquer strategy. Such approaches employ hydropathy scales (or scoring functions; 104–108), which assign an index (or score) to an amino acid residue based on some measure of its aversion to water (e.g., its transfer free energy from oil); the hydrophobicity of a protein patch is then estimated as a sum of the hydrophobicities of constituent amino acids. Numerous hydropathy scales exist, and they can be quite different from one another (109). Importantly, they tend to fare poorly in predicting the driving forces for hydrophobic interactions and assemblies (110–112). The failure of such additive approaches stems not from an imperfect hydropathy scale or scoring function but rather from the underlying assumption that each residue has a unique hydrophobicity. As the examples provided in this section highlight, the collective and nontrivial response of protein hydration waters to the chemical and topographical cues presented by a protein surface means that the hydrophobicity of a residue is not unique but depends sensitively on the context in which it appears on the protein surface.

5. HYDROPHOBIC INTERACTIONS AND ASSEMBLIES: DRIVING FORCES

The association of hydrophobic solutes, which minimizes their disruption of water structure, forms the basis for diverse processes, ranging from micelle formation and protein folding to biomolecular interactions and colloidal assemblies (113–118). The thermodynamic driving forces for such interactions and assemblies depend on the extent to which the solutes disrupt water structure (relative to their assemblies), which in turn, depends sensitively on solute (and assembly) characteristics, such as size, shape, curvature, and chemical patterning (Section 4). Indeed, as described below, differences in the hydration of small and large hydrophobic solutes (Section 2) alone can spawn a veritable menagerie of assembly physics.

5.1. Assemblies of Small Solutes

Molecular self-assembly often involves subnanometer building blocks, which come together to form assemblies that are larger than 1 nm in size, e.g., the association of amphiphilic surfactant molecules to form micelles or the folding of proteins into their native structures (**Figure 4a**). Due to their different sizes, molecular solutes and their assemblies perturb water structure differently. Thus, the hydration free energies, $G_{\rm hyd}$, of individual solutes scale with their volumes, whereas the hydration free energy of the assembly scales as its surface area (Section 2). The driving force for assembling n small solutes into a large aggregate is then $\Delta G_{\rm agg} \approx c \gamma n^{2/3} - n G_{\rm hyd}$, where c depends on aggregate shape. For sufficiently large n, the second term can dominate, so that $\Delta G_{\rm agg}$ depends primarily on solute hydrophobicity, as quantified by $G_{\rm hyd}$. For example, $G_{\rm hyd}$ for surfactant molecules increases linearly with the length of their nonpolar tails (13); correspondingly, the driving force for micelle formation increases with tail length and results in an exponential decrease in the critical micelle concentration (CMC).

The differences in how small solutes and their assemblies perturb water structure are also responsible for the peculiar strengthening of hydrophobic interactions with increasing temperature. In particular, as temperature is increased, G_{hyd} increases, whereas γ decreases (Section 2); consequently, the difference between the two, which represents the driving force for assembly, increases with temperature (14). Indeed, experiments on a variety of surfactants have shown that, at ambient conditions, their CMC goes down as temperature is increased (119), confirming that micelle formation is favored at higher temperatures (**Figure 4b**). Similarly, the stability of folded proteins also increases with temperature near ambient conditions (120, 124, 125). As temperature is increased further, protein stability eventually decreases as the conformational entropy gain upon unfolding

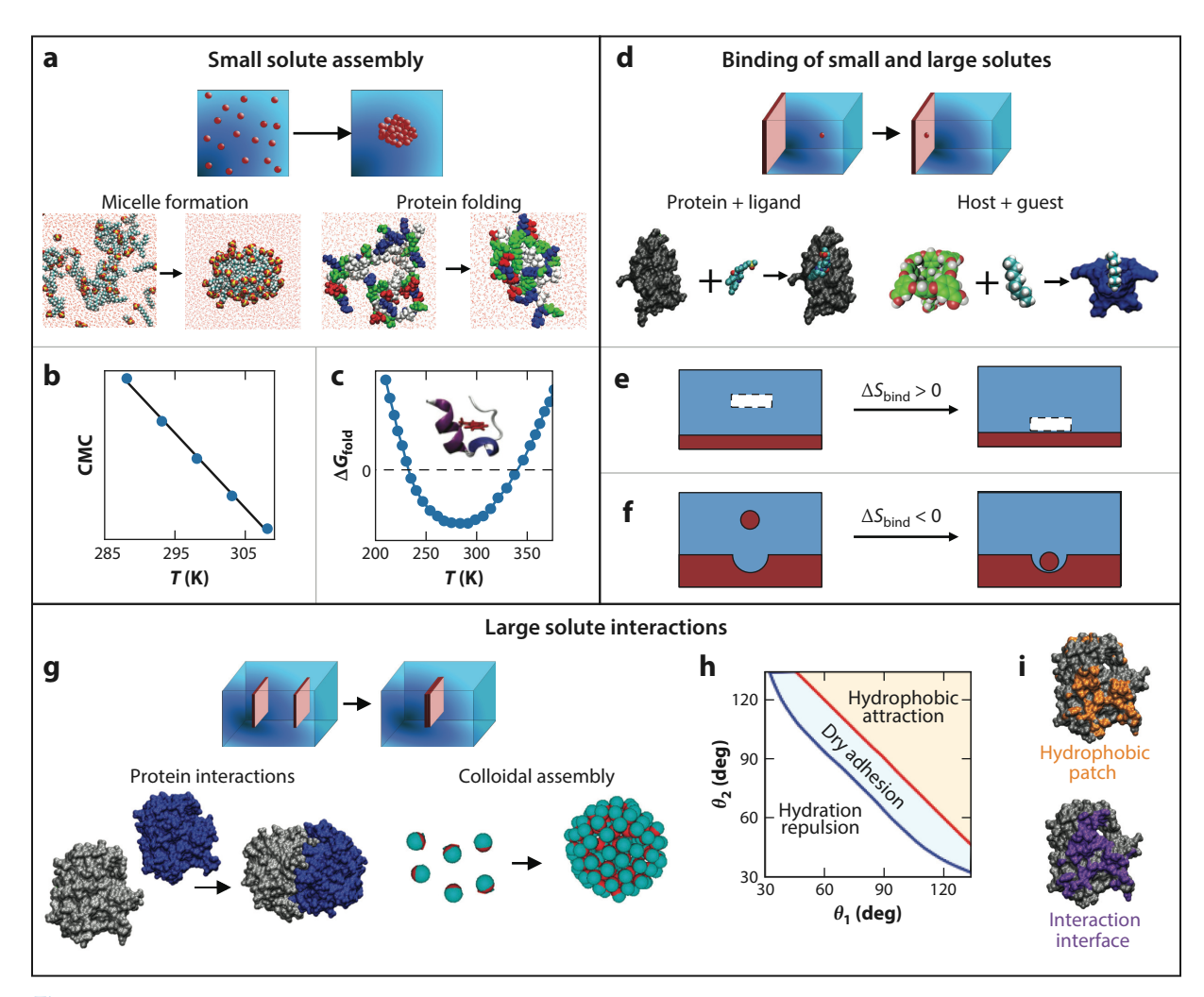


Figure 4

Thermodynamic forces that drive hydrophobic interactions and assemblies. (a) The association of small, hydrophobic solutes plays a role in micelle formation (*left*) and protein folding (*right*). Near ambient conditions, the hydrophobic driving force becomes stronger with increasing temperature, leading to a decrease in (b) the CMC of dodecyl trimethyl ammonium chloride and (c) the folding free energy of the Trp-cage miniprotein. (d) Protein-ligand binding (left) and host-guest interactions (right) involve the association of small hydrophobic solutes with extended surfaces (94, 121). (e) The binding of a hard solute (or cavity) to a hydrophobic surface is favored by entropy (17), whereas (f) the binding of methane to a concave pocket is opposed by entropy (122). (g) Interactions between extended hydrophobic solutes play an important role in protein interactions (left) and colloidal assemblies (right; 123). (b) Kanduč & Netz (29) studied the interactions between extended surfaces with widely varying polarities and found that hydrophobic surfaces were attracted to one another, whereas hydrophilic surfaces experienced hydration repulsion; a weakly attractive regime was observed for intermediate polarities. (i) Rego et al. (30) showed that the most hydrophobic patch of the thymidylate synthase protein, which dewets readily in response to an unfavorable potential, has significant overlap with its interaction interface. Panel b adapted with permission from Reference 119; copyright 2005 Elsevier. Panel c adapted with permission from Reference 120; copyright 2016 National Academy of Sciences. In panel d (right), the teal guest and blue forms are adapted with permission from Reference 121; copyright 2017 American Chemical Society. Also in panel d (right), the green host form is adapted with permission from Reference 94; copyright 2020 Springer Nature. Panel g (right) adapted with permission from Reference 123; copyright 2015 American Institute of Physics. Panel h adapted with permission from Reference 29; copyright 2015 National Academy of Sciences. Panel i adapted with permission from Reference 30; copyright 2021 National Academy of Sciences. Abbreviation: CMC, critical micelle concentration.

prevails over the entropy loss due to hydrophobic hydration. Thus, folded proteins undergo denaturation upon both cooling and heating, albeit for very different reasons (**Figure 4***c*; 126).

5.2. Binding of Small Solutes to Large Solutes

The interactions between subnanometer solutes and those that are larger form the basis for numerous interesting phenomena, including protein–ligand binding and supramolecular chemistry (**Figure 4d**). When a small nonpolar solute binds a hydrophobic surface, water can no longer hydrogen bond around the solute; binding is thus accompanied by the release of constrained hydration waters and ought to be favored by entropy (**Figure 4e**; 17). However, the thermodynamic signatures of such processes can be sensitive to the binding context (38, 127). For example, Setny et al. (122) found that the binding of methane to a concave pocket was favored by enthalpy, rather than entropy. In particular, the release of methane's hydration waters did not drive binding as much as the dewetting of the pocket (**Figure 4f**). Indeed, the favorable dewetting of the pocket is consistent with the observation that concave nonpolar regions are particularly hydrophobic (Section 4.2; **Figure 3b**; 24). A series of experimental studies, which employed isothermal titration calorimetry to characterize the thermodynamics of supramolecular host–guest interactions (128) and protein–ligand binding (129), have similarly highlighted that the affinity of small and large solutes for one another, and in particular, whether binding is driven by enthalpy or entropy, can be remarkably sensitive to small changes in the properties of either solute.

5.3. Interactions Between Extended Solutes

The favorable interactions between extended hydrophobic surfaces drive diverse biomolecular and colloidal assemblies (69; Figure 4g). In contrast with molecular solutes, the driving force for assembling extended surfaces is governed by interfacial physics and decreases with increasing temperature (17). Furthermore, when two surfaces bind, not only are surface-water interactions disrupted but they are replaced by direct interactions between the surfaces. The strength of the former depends on surface hydrophobicity, as quantified by θ (Section 3.2) or G_{cav} (Section 3.4), but the latter can also influence the overall interactions between surfaces. To clarify the interplay between such solvent-mediated and direct interactions, Kanduč & Netz (29) quantified the overall binding strength between two planar surfaces spanning a wide range of polarities (Figure 4b). The authors found that the binding of nonpolar surfaces is highly favorable and is driven by their unfavorable interactions with water. Conversely, the binding of both moderately and strongly polar surfaces was found to be unfavorable in spite of the favorable direct interactions between the surfaces; it turns out that the surfaces interact more favorably with water than with one another, which gives rise to a net repulsion between them. Finally, the authors observed favorable binding between nearly neutral-wetting surfaces over a narrow range of surface polarities; in such a dry adhesion regime, favorable direct interactions between the surfaces are able to edge out favorable surface-water interactions. Interestingly, binding driven by unfavorable surface-water interactions (hydrophobic attraction) spans a much larger range of surface polarities than binding driven by favorable direct interactions between the surfaces (dry adhesion).

5.4. Protein Hydrophobicity Informs Protein Interaction Interfaces

Protein-protein interactions play a crucial role in numerous biological processes and are believed to be driven, at least in part, by hydrophobic interactions (115). Indeed, the findings of Kanduč & Netz (29) suggest that identifying hydrophobic protein regions should provide a promising approach for uncovering the interfaces through which proteins interact (130, 131).

However, identifying hydrophobic protein patches is challenging because protein surfaces are heterogeneous, and their hydrophobicity depends in nontrivial ways on the nanoscale chemical and topographical patterns they display (132, 133; Section 4). To address this challenge, Rego et al. (30) applied an unfavorable potential to all the protein hydration waters; the protein regions that nucleated cavities most readily in response to the potential were then deemed as the most hydrophobic. By comparing these protein regions against experimentally determined protein–protein interaction interfaces, the authors further showed that the most hydrophobic protein patches were also likely to mediate their interactions (**Figure 4***i*); such a correspondence is quite remarkable and points to the importance of hydrophobicity in driving protein interactions.

6. DEWETTING AND BARRIERS TO ASSEMBLY

For nonpolar solutes in water to self-assemble, solute—water interactions must be disrupted. Barriers to assembly thus depend on the ease of dewetting the region between hydrophobic solutes. Solute (de)hydration thus dictates not just the thermodynamics but also the mechanistic pathways and kinetics of assembly (34, 134).

6.1. Barriers to Small Solute Assemblies

The potential of mean force for the association of small hydrophobic solutes, which represents the dependence of free energy on the separation between solutes, displays two minima: a stable contact minimum and a metastable solvent-separated minimum, which are separated by a desolvation barrier (Figure 5a; 134, 135). Because the assembly of small hydrophobic solutes is driven by the release of their constrained hydration waters (Section 5.1), the contact minimum is favored by entropy (136, 137). In contrast, the solvent-separated minimum is favored by enthalpy and disfavored by entropy, owing to the highly constrained hydrogen bonding network of the hydration waters that are shared by the solutes. Many of these constrained hydration waters are released as the system approaches the desolvation barrier, so the barrier configuration is favored by entropy, and its height decreases with increasing temperature. Desolvation barriers can also hinder the favorable interactions between well-hydrated hydrophobic subunits of flexible molecules (e.g., polymer side chains or protein residues), which can drive the conformational transitions of such macromolecules (e.g., polymer collapse or protein folding). Indeed, mechanistic studies of the coil-to-globule transition have shown that the bottleneck to hydrophobic polymer collapse is the formation and dewetting of a sufficiently large nonpolar cluster with water density fluctuations playing an important role in stabilizing the cluster (31, 36, 138; **Figure 5b**).

6.2. Assembly at Hydrophobic Surfaces is Barrierless

Hydrophobic solutes, from noble gases and oils to polymers and proteins, tend to adsorb to hydrophobic surfaces; localized at the surface, these solutes can nevertheless interact with one another and undergo assembly and disassembly. Vembanur et al. (134) showed that desolvation barriers, which impede the assembly of small nonpolar solutes in bulk water, are significantly reduced near an extended hydrophobic surface owing to the relative ease with which its interfacial waters can be displaced (**Figure 5**c). Correspondingly, the kinetics of hydrophobic contact formation (and breakage) were found to be faster near hydrophobic surfaces, suggesting that such surfaces can generically catalyze the assembly (and disassembly) of small hydrophobic solutes. Indeed, Jamadagni et al. (139) showed that nonpolar polymers, which tend to adopt globular conformations in bulk water, instead form pancake-like structures with enhanced conformational

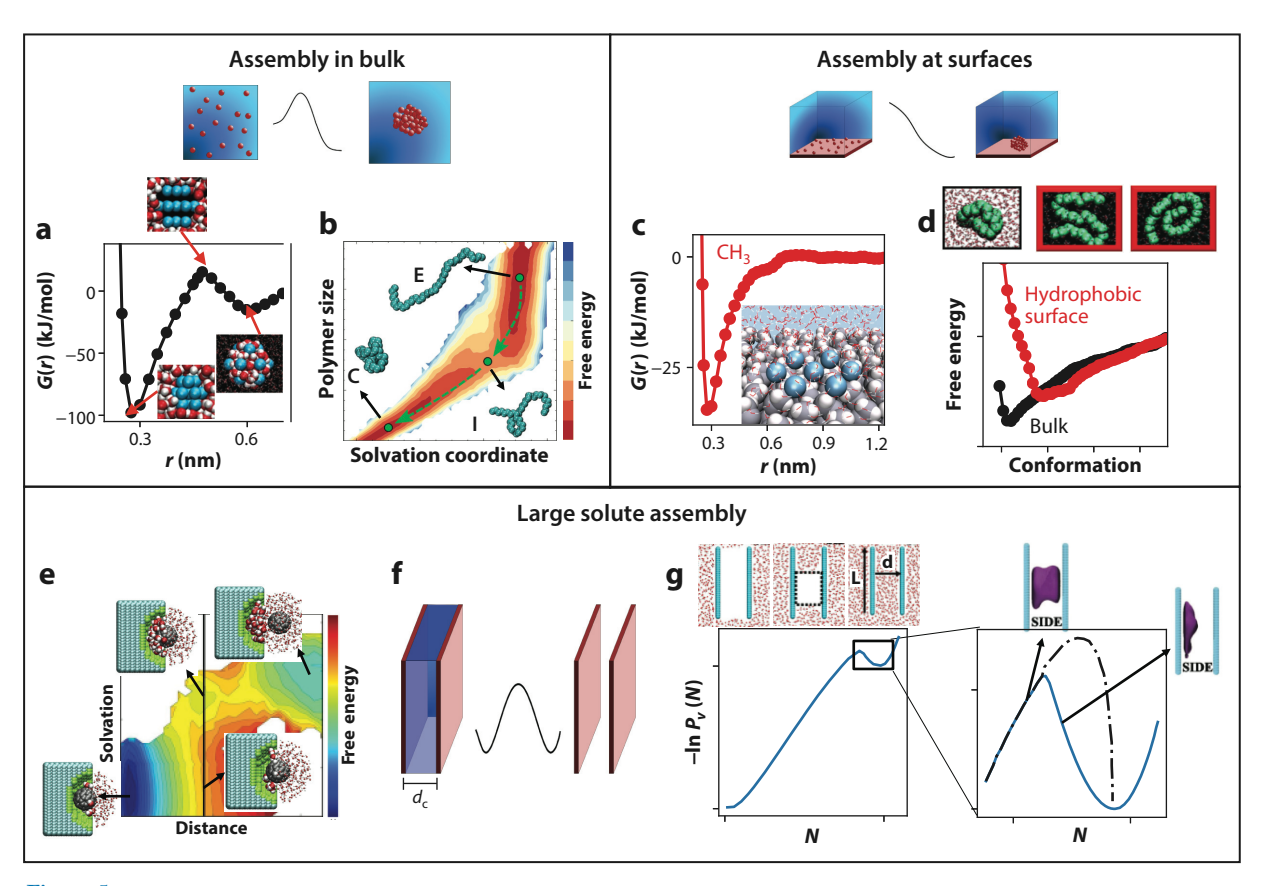


Figure 5

Desolvation barriers to assembly. (a) The potential of mean force for the association of small hydrophobic solutes (cyan) in water (red, white) features a stable contact minimum, a metastable solvent separated minimum, and a desolvation barrier separating the two basins. (b) The free-energy landscape corresponding to the collapse of a hydrophobic polymer in water is shown as a function of the number of waters in its hydration shell, N_v , and the polymer radius of gyration, R_g ; the landscape highlights that an intermediate (I), partially dewetted configuration represents the barrier to the transition from an extended (E) to a collapsed (C) state. (c) In contrast with the assembly in bulk water, the assembly of small hydrophobic solutes at an extended hydrophobic surface is barrierless. (d) Consequently, a hydrophobic polymer adsorbed to a hydrophobic surface displays enhanced conformational fluctuations. (e) The free-energy landscape of fullerene binding to a nonpolar cavity is shown as a function of the separation between the binding partners and the solvation of the cavity; slow solvent fluctuations between wet and dry cavity states (seen at intermediate separations) impede the kinetics of assembly. (f) Although water confined between extended hydrophobic surfaces becomes metastable below a critical separation, d_c , dewetting can be hindered by large free-energy barriers at separations well below dc. (g) Dewetting in confinement between extended hydrophobic surfaces (cyan) is facilitated by water density fluctuations, which nucleate isolated interfacial cavities (purple) adjacent to one of the surfaces (right); the isolated cavities then give way to a plate-spanning vapor tube (left), which can be larger than the critical vapor tube predicted by interfacial physics (dot-dashed line). Panels a and c adapted with permission from Reference 134; copyright 2013 American Chemical Society. Panel b adapted with permission from Reference 36; copyright 2021 American Chemical Society. Panel d adapted with permission from Reference 139; copyright 2009 American Chemical Society. In panel e, the energy landscape is adapted with permission from Reference 34; copyright 2015 National Academy of Sciences. Also in panel ε, the simulation snapshots of the hostguest system are adapted with permission from Reference 143; copyright 2020 American Institute of Physics. Panel g adapted with permission from Reference 144; copyright 2015 National Academy of Sciences.

fluctuations when adsorbed onto hydrophobic surfaces (**Figure 5***d*). Extended hydrophobic surfaces have also been shown to facilitate protein unfolding and subsequent amyloid fibril formation (140, 141).

6.3. Dewetting Barriers Impede the Interactions of Large Solutes

The binding of either small or large hydrophobic solutes to extended hydrophobic surfaces is important in diverse contexts, ranging from protein interactions to nanoparticle self-assembly. A number of studies have investigated the kinetics and mechanistic pathways of such processes and highlighted that binding is hindered by dewetting barriers (32–34, 142). In particular, when two hydrophobic solutes approach one another, water confined between them becomes metastable with respect to its vapor (5); the resulting bistability leads to slow solvent fluctuations between wet and dry states, and thereby to slow binding kinetics (**Figure 5e**). In studying the binding of methane to a hydrophobic pocket, Setny et al. (32) found that a substantial increase in a position-dependent friction coefficient (as methane approached the pocket) was needed to explain the slow binding kinetics. Similarly, in their studies of fullerene binding to a hydrophobic pocket, Mondal et al. (33) found that considering both the ligand–pocket separation and water density in confinement provided a better description of the kinetics of hydrophobic assembly. Studying the same system, Tiwary et al. (34) found that relaxing steric constraints on the fullerene resulted in faster binding kinetics due to a lowering of the associated dewetting barriers.

6.4. Dewetting in Hydrophobic Confinement

Given its role in impeding assembly, the dewetting of the region between two hydrophobic surfaces, fixed at a particular distance from one another, has been studied extensively (145-150). According to classical interfacial physics, the distance between the hydrophobic solutes, d_c , below which water confined between the surfaces becomes metastable with respect to its vapor (**Figure 5**f), is proportional to solute size for nanoscopic solutes and asymptotes to roughly 1.5 µm for macroscopic solutes (37, 151). Furthermore, the bottleneck to dewetting corresponds to the formation of a vapor tube, which spans the region between the surfaces (152–154; Figure 5g). Remsing et al. (144) investigated the role of water density fluctuations in nucleating such vapor tubes and found that enhanced fluctuations near hydrophobic surfaces stabilize isolated cavities adjacent to one or both confining surfaces, which then grow or coalesce to form vapor tubes; furthermore, the nascent vapor tubes can be larger than the critical vapor tubes predicted by interfacial physics. Importantly, such a nonclassical pathway, which circumvents the critical vapor tube, results in a lower barrier to dewetting. Such nonclassical dewetting pathways with smaller dewetting barriers have also been observed in the Wenzel-to-Cassie transition on rough hydrophobic surfaces (155-157) and have facilitated the design of textured surfaces that can undergo barrierless dewetting and spontaneously recover their superhydrophobicity (158).

7. FUTURE OUTLOOK

The origins of our contemporary understanding of hydrophobic effects can be traced back to conceptual breakthroughs in the theory of liquids made more than 50 years ago by Widom, Stillinger, and others (58, 159, 160). Indeed, many of the early insights into these fascinating phenomena were due to theoretical advances (e.g., scaled particle theory, Pratt–Chandler theory, information theory, Lum–Chandler–Weeks theory, etc.), which focused on idealized nonpolar solutes (45, 56, 58, 59). Concurrently, experiments focused on investigating manifestations of hydrophobic effects on more complex solutes, such as proteins, and were harder to interpret using theory (129, 161).

The combination of recent theoretical, simulation, and experimental advances, described here, are beginning to bridge the divide between experiments and theory (39, 40); creative experiments are now being carried out on simpler, more idealized systems (48, 67, 93), and molecular simulations are making it possible to investigate the implications of hydrophobic effects on more and more complex systems, from clay minerals and metals to patterned surfaces and proteins (24, 162, 163). These synergistic advances are poised to deliver exciting breakthroughs in biophysics, soft materials, and beyond.

Predicting the hydrophobicity of heterogeneous surfaces, using schemes that are both highly efficient and sufficiently accurate to predict binding affinities, has been a holy grail for both biophysics and soft materials design (75, 112). The ability to accurately characterize the hydrophobicity of complex surfaces with nanoscale heterogeneity, facilitated by an understanding of interfacial water density fluctuations (Section 3), represents a necessary and important first step in this direction (17, 18). Furthermore, we now understand why well-intentioned prior efforts in this direction, such as the quest for an optimal hydropathy scale, were confounded—the hydrophobicity on a heterogeneous surface depends sensitively on its curvature and chemical patterning (Section 4; 24). In spite of the fact that the relationship between the hydrophobicity of a surface and its chemical and topographical features is both incredibly complex and high dimensional, recent advances in data science may nevertheless provide the requisite framework for capturing such a relationship (85, 164). In particular, a sufficiently large and appropriately curated library of diverse heterogeneous surfaces and/or proteins, whose context-dependent hydrophobicity has been characterized using enhanced sampling techniques or high-throughput experiments, could be used to train a supervised machine learning model.

Learning the complex relationship between the hydrophobicity of a surface and its chemical and topographical patterns could facilitate the design of nanostructured surfaces with bespoke hydrophobicity. For example, the identification of chemical patterns, which confer heterogeneous surfaces with superhydrophilicity, i.e., exceedingly strong interactions with water, could facilitate the discovery of surfaces that resist fouling and are superoleophobic underwater (165). The ability to characterize the hydrophobicity of proteins and an appreciation of its role in driving protein interactions and assemblies (Section 5; 30) has also set the stage for identifying aggregation-prone protein regions and engineering proteins with enhanced solubility (166, 167). Furthermore, an understanding of the role of water density fluctuations in hindering assembly (Section 6), e.g., in protein folding or supramolecular host–guest interactions, could pave the way for engineering assembly pathways and exercising control over the kinetics of assembly (34–36). Finally, an understanding of dewetting pathways in hydrophobic confinement could also facilitate the rational design of textured hydrophobic materials that are capable of dewetting spontaneously, even under hydrostatic pressure, thereby paving the way for their use underwater and in condensation heat transfer (158).

DISCLOSURE STATEMENT

The authors are not aware of any affiliations, memberships, funding, or financial holdings that might be perceived as affecting the objectivity of this review.

ACKNOWLEDGMENTS

A.J.P. gratefully acknowledges financial support from the National Science Foundation (CBET 1652646, CHE 1665339, and UPENN MRSEC DMR 1720530) and awards from the Alfred P. Sloan Research Foundation (FG-2017-9406) and the Camille and Henry Dreyfus Foundation (TC-19-033). N.B.R. was supported by the National Science Foundation, grant numbers

DMR 1844514 and CHE 1665339. The authors thank Jagannath Mondal, Richard Remsing, and Pratyush Tiwary for their feedback on an early version of the manuscript. A.J.P. is grateful for numerous insightful discussions with Shekhar Garde and Hank Ashbaugh.

LITERATURE CITED

- 1. Ball P. 2008. Chem. Rev. 108(1):74-108
- 2. Jamadagni SN, Godawat R, Garde S. 2011. Annu. Rev. Chem. Biomol. Eng. 2:147-71
- 3. Hillyer MB, Gibb BC. 2016. Annu. Rev. Phys. Chem. 67:307-29
- 4. Ben-Amotz D. 2016. Annu. Rev. Phys. Chem. 67:617-38
- 5. Berne BJ, Weeks JD, Zhou R. 2009. Annu. Rev. Phys. Chem. 60:85-103
- 6. Dill KA, Truskett TM, Vlachy V, Hribar-Lee B. 2005. Annu. Rev. Biophys. Biomol. Struct. 34:173-99
- 7. Tanford C. 1973. Hydrophobic Effect: Formation of Micelles and Biological Membranes. New York: Wiley
- 8. Haase MF, Sharifi-Mood N, Lee D, Stebe KJ. 2016. ACS Nano 10(6):6338-44
- 9. Dobson CM. 2003. Nature 426(6968):884-90
- 10. Levy Y, Onuchic JN. 2006. Annu. Rev. Biophys. Biomol. Struct. 35:389-415
- 11. Krone MG, Hua L, Soto P, Zhou R, Berne BJ, Shea JE. 2008. 7. Am. Chem. Soc. 130(33):11066-72
- 12. Thirumalai D, O'Brien EP, Morrison G, Hyeon C. 2010. Annu. Rev. Biophys. 39:159–83
- Chandler D, Varilly P. 2012. Proc. Int. School Phys. "Enrico Fermi", Vol. 176, Complex Materials in Physics and Biology, Varenna, Italy, July 2010, ed. F Mallamace, HE Stanley, pp. 75–111. Amsterdam: IOS Press
- 14. Chandler D. 2005. Nature 437(7059):640–47
- 15. Godawat R, Jamadagni SN, Garde S. 2009. PNAS 106(36):15119-24
- 16. Patel AJ, Varilly P, Chandler D. 2010. 7. Phys. Chem. B 114(4):1632-37
- 17. Patel AJ, Varilly P, Jamadagni SN, Acharya H, Garde S, Chandler D. 2011. PNAS 108(43):17678-83
- Patel AJ, Varilly P, Jamadagni SN, Hagan MF, Chandler D, Garde S. 2012. J. Phys. Chem. B 116(8):2498– 503
- 19. Patel AJ, Garde S. 2014. J. Phys. Chem. B 118(6):1564-73
- 20. Giovambattista N, Lopez CF, Rossky PJ, Debenedetti PG. 2008. PNAS 105(7):2274–79
- 21. Giovambattista N, Debenedetti PG, Rossky PJ. 2009. PNAS 106(36):15181-85
- 22. Acharya H, Vembanur S, Jamadagni SN, Garde S. 2010. Faraday Discuss. 146:353-65
- 23. Mittal J, Hummer G. 2010. Faraday Discuss. 146:341–52
- 24. Xi E, Venkateshwaran V, Li L, Rego N, Patel AJ, Garde S. 2017. PNAS 114(51):13345-50
- 25. Fennell CJ, Dill KA. 2011. J. Stat. Phys. 145(2):209-26
- 26. Harris RC, Pettitt BM. 2014. PNAS 111(41):14681-86
- 27. Wang J, Bratko D, Luzar A. 2011. PNAS 108(16):6374-79
- 28. Factorovich MH, Molinero V, Scherlis DA. 2015. 7. Am. Chem. Soc. 137(33):10618–23
- 29. Kanduč M, Netz RR. 2015. PNAS 112(40):12338-43
- 30. Rego NB, Xi E, Patel AJ. 2021. PNAS 118(6):e2018234118
- 31. Miller TF, Vanden-Eijnden E, Chandler D. 2007. PNAS 104(37):14559–64
- 32. Setny P, Baron R, Kekenes-Huskey PM, McCammon JA, Dzubiella J. 2013. PNAS 110(4):1197-202
- 33. Mondal J, Morrone JA, Berne BJ. 2013. PNAS 110(33):13277-82
- 34. Tiwary P, Mondal J, Morrone JA, Berne BJ. 2015. PNAS 112(39):12015-19
- 35. Jiang Z, Remsing RC, Rego NB, Patel AJ. 2019. 7. Phys. Chem. B 123(7):1650-61
- 36. Dhabal D, Jiang Z, Pallath A, Patel AJ. 2021. 7. Phys. Chem. B 125(20):5434-42
- 37. Giovambattista N, Rossky P, Debenedetti P. 2012. Annu. Rev. Phys. Chem. 63:179-200
- 38. Baron R, McCammon JA. 2013. Annu. Rev. Phys. Chem. 64:151–75
- Bellissent-Funel MC, Hassanali A, Havenith M, Henchman R, Pohl P, et al. 2016. Chem. Rev. 116(13):7673–97
- Monroe J, Barry M, DeStefano A, Aydogan Gokturk P, Jiao S, et al. 2020. Annu. Rev. Chem. Biomol. Eng. 11:523–57
- 41. Hummer G, Garde S, García AE, Paulaitis ME, Pratt LR. 1998. J. Phys. Chem. B 102(51):10469-82
- 42. Southall NT, Dill KA, Haymet ADJ. 2002. J. Phys. Chem. B 106(3):521-33

- 43. Lee CY, McCammon JA, Rossky PJ. 1984. 7. Chem. Phys. 80(9):4448-55
- 44. Willard AP, Chandler D. 2010. 7. Phys. Chem. B 114(5):1954-58
- 45. Hummer G, Garde S, García AE, Pohorille A, Pratt LR. 1996. PNAS 93(17):8951-55
- 46. Garde S, Hummer G, García AE, Paulaitis ME, Pratt LR. 1996. Phys. Rev. Lett. 77(24):4966-68
- 47. Patel AJ, Varilly P, Chandler D, Garde S. 2011. 7. Stat. Phys. 145(2):265-75
- 48. Li ITS, Walker GC. 2011. PNAS 108(40):16527–32
- 49. Remsing RC, Patel AJ. 2015. J. Chem. Phys. 142(2):024502
- 50. Weeks JD. 2002. Annu. Rev. Phys. Chem. 53:533-62
- 51. Ashbaugh HS, Pratt LR. 2006. Rev. Mod. Phys. 78(1):159-78
- 52. Remsing RC, Weeks JD. 2013. 7. Phys. Chem. B 117(49):15479-91
- 53. Widom B. 1963. 7. Chem. Phys. 39(11):2808-12
- 54. Beck TL, Paulaitis ME, Pratt LR. 2006. The Potential Distribution Theorem and Models of Molecular Solutions. Cambridge, UK: Cambridge Univ. Press
- 55. Chandler D. 1993. Phys. Rev. E 48(4):2898-905
- 56. Pratt LR, Chandler D. 1977. J. Chem. Phys. 67(8):3683-704
- 57. Pratt LR. 2002. Annu. Rev. Phys. Chem. 53:409-36
- 58. Stillinger FH. 1973. J. Solut. Chem. 2(2):141-58
- 59. Lum K, Chandler D, Weeks JD. 1999. J. Phys. Chem. B 103(22):4570-77
- 60. Huang DM, Chandler D. 2000. PNAS 97(15):8324-27
- 61. Huang DM, Geissler PL, Chandler D. 2001. J. Phys. Chem. B 105(28):6704-9
- 62. Rajamani S, Truskett TM, Garde S. 2005. PNAS 102(27):9475-80
- 63. ten Wolde PR, Sun SX, Chandler D. 2002. Phys. Rev. E 65(1 Pt. 1):011201
- 64. Varilly P, Patel AJ, Chandler D. 2011. J. Chem. Phys. 134(7):074109
- 65. Vaikuntanathan S, Rotskoff G, Hudson A, Geissler PL. 2016. PNAS 113(16):E2224-30
- 66. Xi E, Patel AJ. 2016. PNAS 113(17):4549-51
- 67. Davis JG, Gierszal KP, Wang P, Ben-Amotz D. 2012. Nature 491(7425):582-85
- 68. Garde S, Patel AJ. 2011. PNAS 108(40):16491-92
- Israelachvili J, Wennerström H. 1996. Nature 379(6562):219–25
- 70. Ben-Naim A. 1978. J. Phys. Chem. 82(7):792–803
- 71. Ben-Naim A. 1987. Solvation Thermodynamics. New York: Springer
- 72. Beglov D, Roux B. 1994. 7. Chem. Phys. 100(12):9050-63
- 73. Jiang H, Patel AJ. 2019. Curr. Opin. Chem. Eng. 23:130-37
- 74. Jiang H, Fialoke S, Vicars Z, Patel AJ. 2019. Soft Matter 15(5):860-69
- 75. Granick S, Bae SC. 2008. Science 322(5907):1477-78
- 76. Mittal J, Hummer G. 2008. PNAS 105(51):20130–35
- 77. Sarupria S, Garde S. 2009. Phys. Rev. Lett. 103(3):037803
- 78. Laage D, Stirnemann G, Sterpone F, Hynes JT. 2012. Acc. Chem. Res. 45(1):53-62
- 79. Shenogina N, Godawat R, Keblinski P, Garde S. 2009. Phys. Rev. Lett. 102(15):156101
- 80. Ajdari A, Bocquet L. 2006. Phys. Rev. Lett. 96(18):186102
- 81. Giovambattista N, Debenedetti PG, Rossky PJ. 2007. J. Phys. Chem. C 111(3):1323-32
- 82. Heyden M, Tobias DJ. 2013. Phys. Rev. Lett. 111(21):218101
- 83. Fogarty AC, Laage D. 2014. 7. Phys. Chem. B 118(28):7715-29
- 84. Shin S, Willard AP. 2018. J. Phys. Chem. B 122(26):6781–89
- 85. Monroe JI, Shell MS. 2018. PNAS 115(32):8093-98
- 86. Heyden M. 2019. WIREs Comput. Mol. Sci. 9(2):e1390
- 87. Xiao Q, Liu Y, Guo Z, Liu Z, Lohse D, Zhang X. 2017. Langmuir 33(32):8090-96
- 88. Xi E, Remsing RC, Patel AJ. 2016. J. Chem. Theory Comput. 12(2):706-13
- 89. Young T, Abel R, Kim B, Berne BJ, Friesner RA. 2007. PNAS 104(3):808-13
- 90. Nguyen CN, Kurtzman Young T, Gilson MK. 2012. 7. Chem. Phys. 137(4):044101
- 91. Huggins DJ, Payne MC. 2013. J. Phys. Chem. B 117(27):8232-44
- 92. Levy RM, Cui D, Zhang BW, Matubayasi N. 2017. 7. Phys. Chem. B 121(15):3825-41
- 93. Ma CD, Wang C, Acevedo-Vélez C, Gellman SH, Abbott NL. 2015. Nature 517(7534):347-50

- 94. Barnett JW, Sullivan MR, Long JA, Tang D, Nguyen T, et al. 2020. Nat. Chem. 12(7):589-94
- 95. Garde S. 2015. Nature 517(7534):277-79
- 96. Garde S. 2020. Nat. Chem. 12(7):587-88
- 97. Zhou R, Huang X, Margulis CJ, Berne BJ. 2004. Science 305(5690):1605-9
- 98. Liu P, Huang X, Zhou R, Berne BJ. 2005. Nature 437(7055):159-62
- 99. Rego NB, Xi E, Patel AJ. 2019. J. Am. Chem. Soc. 141(5):2080-86
- 100. Eisenberg D, McLachlan AD. 1986. Nature 319(6050):199-203
- 101. Roux B, Simonson T. 1999. Biophys. Chem. 78(1-2):1-20
- 102. Kang YK, Nemethy G, Scheraga HA. 1987. J. Phys. Chem. 91(15):4105-9
- 103. Mobley DL, Bayly CI, Cooper MD, Shirts MR, Dill KA. 2009. 7. Chem. Theory Comput. 5(2):350-58
- 104. Kyte J, Doolittle RF. 1982. 7. Mol. Biol. 157(1):105-32
- 105. Ferrara P, Gohlke H, Price DJ, Klebe G, Brooks CL. 2004. 7. Med. Chem. 47(12):3032-47
- 106. Bonella S, Raimondo D, Milanetti E, Tramontano A, Ciccotti G. 2014. 7. Phys. Chem. B 118(24):6604-13
- 107. Eisenberg D. 1984. Annu. Rev. Biochem. 53:595-623
- 108. Rose GD, Wolfenden R. 1993. Annu. Rev. Biophys. Biomol. Struct. 22:381-415
- 109. Cornette JL, Cease KB, Margalit H, Spouge JL, Berzofsky JA, DeLisi C. 1987. J. Mol. Biol. 195(3):659-85
- 110. Kortemme T, Baker D. 2002. PNAS 99(22):14116-21
- 111. Kollman PA, Massova I, Reyes C, Kuhn B, Huo S, et al. 2000. Acc. Chem. Res. 33(12):889-97
- 112. Kister AE, Phillips JC. 2008. PNAS 105(27):9233-37
- 113. Shen VK, Cheung JK, Errington JR, Truskett TM. 2006. Biophys. J. 90(6):1949-60
- 114. Palmer JC, Debenedetti PG. 2012. J. Phys. Chem. Lett. 3(18):2713-18
- 115. Thirumalai D, Reddy G, Straub JE. 2012. Acc. Chem. Res. 45(1):83-92
- 116. Vashisth H, Abrams CF. 2013. Proteins: Struct., Funct., Bioinf. 81(6):1017-30
- 117. Remsing RC, Xi E, Patel AJ. 2018. *J. Phys. Chem. B* 122(13):3635–46
- 118. Whitesides GM, Grzybowski B. 2002. Science 295(5564):2418-21
- Mehta SK, Bhasin KK, Chauhan R, Dham S. 2005. Colloids Surf. A 255(1):153–57. https://www.sciencedirect.com/journal/colloids-and-surfaces-a-physicochemical-and-engineering-aspects
- 120. Kim SB, Palmer JC, Debenedetti PG. 2016. PNAS 113(32):8991-96
- 121. Tang D, Barnett JW, Gibb BC, Ashbaugh HS. 2017. 7. Phys. Chem. B 121(47):10717–25
- 122. Setny P, Baron R, McCammon JA. 2010. J. Chem. Theory Comput. 6(9):2866-71
- 123. Avvisati G, Vissers T, Dijkstra M. 2015. 7. Chem. Phys. 142(8):084905
- 124. Tanford C. 1968. Adv. Protein Chem. 23:121-282
- 125. Privalov PL. 1990. Crit. Rev. Biochem. Mol. Biol. 25(4):281-306
- 126. Matysiak S, Debenedetti PG, Rossky PJ. 2012. J. Phys. Chem. B 116(28):8095-104
- 127. Monroe JI, Jiao S, Davis RJ, Brown DR, Katz LE, Shell MS. 2021. PNAS 118(1):e2020205118
- 128. Suating P, Nguyen TT, Ernst NE, Wang Y, Jordan JH, et al. 2020. Chem. Sci. 11(14):3656-63
- 129. Snyder PW, Mecinović J, Moustakas DT, Thomas SW, Harder M, et al. 2011. PNAS 108(44):17889-94
- 130. Young L, Jernigan RL, Covell DG. 1994. Prot. Sci. 3(5):717-29
- 131. Keskin O, Gursoy A, Ma B, Nussinov R. 2008. Chem. Rev. 108(4):1225-44
- 132. Rossky PJ. 2010. Faraday Discuss. 146:13-18
- 133. Cui D, Ou S, Patel S. 2014. Proteins: Struct., Funct., Bioinf. 82(12):3312-26
- 134. Vembanur S, Patel AJ, Sarupria S, Garde S. 2013. 7. Phys. Chem. B 117(35):10261-70
- 135. Pangali C, Rao M, Berne BJ. 1979. J. Chem. Phys. 71(7):2982-90
- 136. Ghosh T, García AE, Garde S. 2002. 7. Chem. Phys. 116(6):2480-86
- 137. Widom B, Bhimalapuram P, Koga K. 2003. Phys. Chem. Chem. Phys. 5(15):3085-93
- 138. ten Wolde PR, Chandler D. 2002. PNAS 99(10):6539-43
- 139. Jamadagni SN, Godawat R, Dordick JS, Garde S. 2009. J. Phys. Chem. B 113(13):4093-101
- 140. Pronchik J, He X, Giurleo JT, Talaga DS. 2010. 7. Am. Chem. Soc. 132(28):9797-803
- 141. Beverung CJ, Radke CJ, Blanch HW. 1999. Biophys. Chem. 81(1):59-80
- 142. Lamim Ribeiro JM, Tiwary P. 2019. J. Chem. Theory Comput. 15(1):708-19
- 143. Ahalawat N, Bandyopadhyay S, Mondal J. 2020. 7. Chem. Phys. 152(7):074104
- 144. Remsing RC, Xi E, Vembanur S, Sharma S, Debenedetti PG, et al. 2015. PNAS 112(27):8181-86

- 145. Huang X, Margulis CJ, Berne BJ. 2003. PNAS 100(21):11953-58
- 146. Choudhury N, Pettitt BM. 2007. 7. Am. Chem. Soc. 129(15):4847-52
- 147. Xu L, Molinero V. 2010. J. Phys. Chem. B 114(21):7320-28
- 148. Sharma S, Debenedetti PG. 2012. PNAS 109(12):4365-70
- 149. Altabet YE, Haji-Akbari A, Debenedetti PG. 2017. PNAS 114(13):E2548-55
- 150. Xi E, Marks SM, Fialoke S, Patel AJ. 2018. Mol. Simul. 44(13-14):1124-35
- 151. Cerdeiriña CA, Debenedetti PG, Rossky PJ, Giovambattista N. 2011. 7. Phys. Chem. Lett. 2(9):1000-3
- 152. Lum K, Luzar A. 1997. Phys. Rev. E 56(6):R6283-86
- 153. Bolhuis PG, Chandler D. 2000. 7. Chem. Phys. 113(18):8154-60
- 154. Leung K, Luzar A, Bratko D. 2003. Phys. Rev. Lett. 90(6):065502
- 155. Quéré D. 2008. Annu. Rev. Mater. Res. 38:71-99
- 156. Papadopoulos P, Mammen L, Deng X, Vollmer D, Butt HJ. 2013. PNAS 110(9):3254-58
- Arunachalam S, Das R, Nauruzbayeva J, Domingues EM, Mishra H. 2019. J. Colloid Interface Sci. 534:156–62
- 158. Prakash S, Xi E, Patel AJ. 2016. PNAS 113(20):5508-13
- 159. Widom B. 1967. Science 157(3787):375-82
- 160. Chandler D. 2017. Annu. Rev. Phys. Chem. 68:19-38
- Kauzmann W. 1959. In Advances in Protein Chemistry, Vol. 14, ed. CB Anfinsen, ML Anson, K Bailey, JT Edsall, pp. 1–63. New York: Academic
- 162. Rotenberg B, Patel AJ, Chandler D. 2011. 7. Am. Chem. Soc. 133:20521-27
- 163. Limmer DT, Willard AP, Madden P, Chandler D. 2013. PNAS 110(11):4200-5
- 164. Kelkar AS, Dallin BC, Van Lehn RC. 2020. 7. Phys. Chem. B 124(41):9103-14
- 165. Chen S, Cao Z, Jiang S. 2009. Biomaterials 30(29):5892-96
- 166. Shire SJ, Shahrokh Z, Liu J. 2004. 7. Pharm. Sci. 93(6):1390-402
- 167. Chong SH, Ham S. 2014. Angew. Chem. Int. Ed. Engl. 53(15):3961-64



Contents

Annual Review of Condensed Matter Physics

Volume 13, 2022

Reflections on 65 Years of Helium Research John D. Reppy	1
My Life and Science Valery L. Pokrovsky	15
Russell Donnelly and His Leaks J.J. Niemela and K.R. Sreenivasan	33
Director Deformations, Geometric Frustration, and Modulated Phases in Liquid Crystals *Jonathan V. Selinger**	49
Thin Film Skyrmionics Takaaki Dohi, Robert M. Reeve, and Mathias Kläui	73
The Physics of Dense Suspensions Christopher Ness, Ryohei Seto, and Romain Mari	97
Topological Magnets: Functions Based on Berry Phase and Multipoles Satoru Nakatsuji and Ryotaro Arita	119
Active Turbulence Ricard Alert, Jaume Casademunt, and Jean-François Joanny	143
Topological Magnons: A Review Paul A. McClarty	171
Olfactory Sensing and Navigation in Turbulent Environments Gautam Reddy, Venkatesh N. Murthy, and Massimo Vergassola	191
Irreversibility and Biased Ensembles in Active Matter: Insights from Stochastic Thermodynamics Étienne Fodor, Robert L. Jack, and Michael E. Cates	215
The Hubbard Model Daniel P. Arovas, Erez Berg, Steven A. Kivelson, and Srinivas Raghu	239
The Hubbard Model: A Computational Perspective Mingpu Qin, Thomas Schäfer, Sabine Andergassen, Philippe Corboz,	275
and Emanuel Gull	4/5

Understanding Hydrophobic Effects: Insights from Water Density Fluctuations Nicholas B. Rego and Amish J. Patel	303
Modeling of Ferroelectric Oxide Perovskites: From First to Second Principles Philippe Ghosez and Javier Junquera	
How Cross-Link Numbers Shape the Large-Scale Physics of Cytoskeletal Materials Sebastian Fürthauer and Michael J. Shelley	365
Studying Quantum Materials with Scanning SQUID Microscopy Eylon Persky, Ilya Sochnikov, and Beena Kalisky	385
Coherently Coupled Mixtures of Ultracold Atomic Gases Alessio Recati and Sandro Stringari	407

Errata

An online log of corrections to *Annual Review of Condensed Matter Physics* articles may be found at http://www.annualreviews.org/errata/conmatphys